Adv. Polar Upper Atmos. Res., **19**, 71–79, 2005

Research note

High-resolution simulation of propagation of interplanetary shock wave caused by a coronal mass ejection observed on November 13, 2003

Tomoya Ogawa[1]*, Mitsue Den[1], Takashi Tanaka[2] and Kazuyuki Yamashita[3]

[1] *Space Simulation Group, National Institute of Information and Communications Technology, Nukuikita-Machi 4–2–1, Koganei-shi, Tokyo 184-8795*
[2] *Department of Earth and Planetary Sciences, Kyushu University, Hakozaki 6–10–1, Higashi-ku, Fukuoka 812-8581*
[3] *The Center for Educational Research, University of Yamanashi, Takeda 4, Kofu 400-8510*
**Corresponding author. E-mail: ogawa@nict.go.jp*

(Received December 18, 2004; Accepted April 12, 2005)

Abstract: We simulated the three-dimensional (3D) propagation of a shock wave caused by a coronal mass ejection (CME) on November 13, 2003. The 3D simulations were performed using a high-resolution adaptive mesh refinement (AMR) technique. The AMR technique enabled us to resolve near the sun with $(0.06R_\odot)^3$-sized cells and to resolve the entire shock front with $(0.24R_\odot)^3$-sized cells in an interplanetary simulation within a $(500R_\odot)^3$-sized computational box. The solar wind was measured by an imaginary spacecraft positioned at point L1 in the simulations. A model fitted for solar wind density fluctuations observed by the ACE spacecraft was employed, and models in which some CME parameters were changed were employed for comparison. The relationships between the CME parameters and the solar wind fluctuations were also investigated, and the results were compared with the solar wind data observed at point L1 by the ACE spacecraft.

key words: coronal mass ejection, interplanetary shock wave, three-dimensional simulation

1. Introduction

Fast coronal mass ejections (CMEs) cause shock waves in interplanetary space. The shock waves may continue to fluctuate strongly when they arrive at Earth, leading to space weather phenomena in the Earth's magnetosphere and ionosphere.

Three-dimensional (3D) simulations of interplanetary shock wave propagation are difficult to perform in one simulation box spanning the orbit of Earth as long as a regular mesh structure is used because of limitations in computational resources (CPU power and memory capacity). The use of a spherical mesh is one effective solution to this problem. Odstrcil and Pizzo (1999) and Odstrcil *et al.* (2004) used a fan-shaped spherical mesh to investigate CME-caused structures within a streamer belt. However, a spherical mesh cannot resolve CME-caused shock waves with a high resolution once

the shock waves are distant from the sun. The use of an adaptive mesh refinement (AMR) technique (Khokhlov, 1998) is an excellent solution to this problem. The AMR technique dynamically adapts the meshes to suit the physical state. Running structures can be monitored using fine meshes and coarse meshes can be allocated to quiet regions. This feature makes it possible to simulate interplanetary shock wave propagations with high resolution. Manchester *et al.* (2004) performed AMR simulations of interplanetary CME propagation, but they localized their fine meshes for the CME to a narrow region along a sun-to-earth line.

We used a 3D AMR hydrodynamic code to simulate an interplanetary shock wave caused by a CME that occurred at 0930 UT on November 13, 2003. The CME was observed by SOHO/LASCO with a velocity of 1141 km/s (see the SOHO LASCO CME Catalog available on the SOHO web page). We selected this CME because it produced a clear shock wave on a quiet solar wind. The relevant shock wave was observed by the ACE spacecraft about 43.8 hours after the detection of the CME. In our simulations, the plane of the shock wave was processed using small cells, and a high resolution was maintained throughout the simulation.

2. Simulation

Simulations of CME-caused shock waves were performed using our 3D AMR code. With the AMR technique, the areas, positions, and shapes of the regions of fine meshes can be adapted to suit the physical state in progress. This makes it possible to monitor the shock wave structure using fine meshes and to monitor the ambient solar wind using coarse meshes, enabling high-resolution simulations to be performed using available computer resources.

The equations for the system are

$$\begin{cases} \dfrac{\partial \rho}{\partial t} + \nabla \cdot (\rho \mathbf{u}) = 0, \\ \dfrac{\partial (\rho \mathbf{u})}{\partial t} + \nabla \cdot (\rho \mathbf{u}\mathbf{u}) = \rho \mathbf{g}, \\ \dfrac{\partial e}{\partial t} + \nabla \cdot (e+P)\mathbf{u} = \rho \mathbf{g} \cdot u + (\gamma - 1)Q, \end{cases} \tag{1}$$

where ρ, $\mathbf{u}$, $\mathbf{g}$, e, P, γ, and Q are mass density, velocity, gravitational acceleration, total energy density, pressure, specific heat ratio, and heating function, respectively. We set

$$\gamma = \frac{5}{3}, \tag{2}$$

and

$$\mathbf{g} = G \frac{M_\odot}{r^3} \mathbf{r}, \tag{3}$$

where G, $M_\odot$, $\mathbf{r}$, and $r \equiv |\mathbf{r}|$ are the gravitational constant, the solar mass, the position vector from the solar center, and the distance from the solar center, respectively. And we set the heating function as

$$Q = -\rho q_0 (T - T_0) \exp\left[- \frac{(r - R_\odot)^2}{\sigma_0^2} \right], \tag{4}$$

where T, r, and $R_\odot$ are temperature, distance from the sun, and the solar radius, respectively. We choose $\sigma_0 = 4.5 R_\odot$, which was the minimum value used by Manchester *et al.* (2004) and

$$\begin{cases} q_0 = 10^6 \text{erg/g/s/K}, \\ T_0 = 2.7 \times 10^6 \text{K}, \end{cases} \tag{5}$$

to reproduce the density and the velocity of the solar wind observed by the ACE spacecraft at point L1. We set the density at the inner boundary to $\rho = 1.3 \times 10^6$ protons/cm^3. The above parameters were used to reproduce the velocity and the density of the solar wind in the pre-shock region.

The equations were then rewritten into difference equations that can be solved using the Roe-MUSCL algorithm (Roe, 1981; Van Leer, 1977, 1979; Fujii, 1994). The size of the computational box was $(500 R_\odot)^3$. The sun was positioned at the conter of the box. The inner boundary was set at $1.1 R_\odot$. The cell size was $(0.06 R_\odot)^3$ near the sun, $(0.24 R_\odot)^3$ in the area of the shock wave, and $(7.8 R_\odot)^3$ for the maximum cells. We first obtain a steady-state solar wind and then inputted the model CME into the inner boundary. The CME model is described in the next section.

3. CME model

Once a steady-state solar wind was produced, we inputted a model CME into the inner boundary. We focused on a CME that occurred at 0930 UT on November 13, 2003. The speed of the CME was measured as 1141 km/s by SOHO/LASCO. We modeled the CME as follows:

$$\begin{cases} A(\xi) = \cos\left(\dfrac{\pi \xi}{2 \xi_0} \right) \\ B(t) = \begin{cases} \dfrac{t}{\tau_r} & (0 < t < \tau_r) \\ 1 & (\tau_r < t < \tau_r + \tau_d) \\ \dfrac{2\tau_r + \tau_d - t}{\tau_r} & (\tau_r + \tau_d < t < 2\tau_r + \tau_d) \end{cases} \\ V(t, \xi) = V_{\max} A(\xi) B(t) \\ \rho(t, \xi) = \rho_{\text{SW}} + \rho_{\text{CME}} A(\xi) B(t), \end{cases} \tag{6}$$

where V_{CME} is the radial velocity of the input CME, $V_{\max}$ is the maximum of V_{CME}, ρ_{SW} is the density of the pre-CME solar wind, ρ_{CME} is the additional density of the input CME, and ξ, ξ_0, τ_r, and τ_d are the angle to the axis of the CME cone, the angular radius of the CME, the stand-up time, and the duration of the CME, respectively (Odstrcil and Pizzo, 1999). We adopted $\xi_0 = 15^\circ$ and $\tau_r = 1$ hour; these values are the ones used by Odstrcil and Pizzo (1999). And we set $V_{\max}$ as the observed CME velocity. The *Joint*

Table 1. Density, duration, position, and mass of the CME in each of the models.

Model	ρ_{CME} (cm^{-3})	τ_d (hour)	Longitude	Mass (g)
1	1.0×10^6	4	E25°	1.1×10^{15}
2	1.0×10^6	4	E15°	1.1×10^{15}
3	2.6×10^6	4	E30°	3.8×10^{15}
4	0.5×10^6	10	E25°	1.7×10^{15}

ρ_{CME}, density; τ_d, duration. All other parameters were fixed, as described in the text.

USAF/NOAA Report of Solar and Geophysical Activity reported that the CME appeared to erupt off an east limb. We therefore assumed that the CME occurred on the east side of the equator. The longitude, together with the ρ_{CME} and τ_d, were adjusted as a temporal plot of the solar wind density at point L1 to fit the ACE data. These fitted values were used in model 1, shown in Table 1. For comparison, we simulated three other models that deviated from the fitted point. Model 2 was the same as model 1 except for the direction of the eruption of the CME. Model 3 had a higher density and the longitude was adjusted so that the density peak at point L1 agreed with the observed value. Model 4 had a longer duration time and the same longitude as model 1. The density of model 4 was adjusted so that the density peak at point L1 agreed with the observed value. These models are summarized in Table 1.

4. Results

The density distributions of model 1 on the solar equator plane at 24 and 52 hours after the CME are shown in Fig. 1. An imaginary spacecraft placed at point L1 in a simulation box was used to observe the time variations of the solar wind. The density and velocity of model 1 are plotted in Fig. 2, together with the ACE data. The density of models 2, 3, and 4 are plotted in Fig. 3, while the velocities of these models are shown in Fig. 4. The upper-left panels of Figs. 3 and 4 are the same as the left and right panels of Fig. 2, respectively. These plots were adjusted so that the rise time of the simulated shocks coincided with the observed one. Shock waves were detected in each model. The arrival times of the shock waves in each model were 51.6, 47.2, 50.2, and 51.6 hours after the beginning of the CME input. A shock wave was seen in the ACE data 43.8 hours after SOHO/LASCO detected a bright loop. Of note, the data were measured at the center of the cell nearest to point L1, not just at point L1. This method produced apparent discontinuities in the temporal plots when the cell size was changed. For instance, the jumps in the post-shock region seen in Figs. 2, 3, and 4 are not real discontinuities. Such jumps were small near the shock front well because the size of the cells near the shock front was small. The density plot of model 1 agreed with the observations, but the peak was somewhat higher. The velocity of model 1 had a somewhat lower peak and was difficult to decrease. Model 2 was the same as model 1, but the erupting direction was turned toward Earth. The density plot of model 2 had a higher peak and a subsequent second peak. The velocity of model 2 was 10^1 km/s higher than that of model 1. Model 3 erupted a larger mass directed away from Earth. The density peak of model 3 moved backward from the shock. The velocity plot of

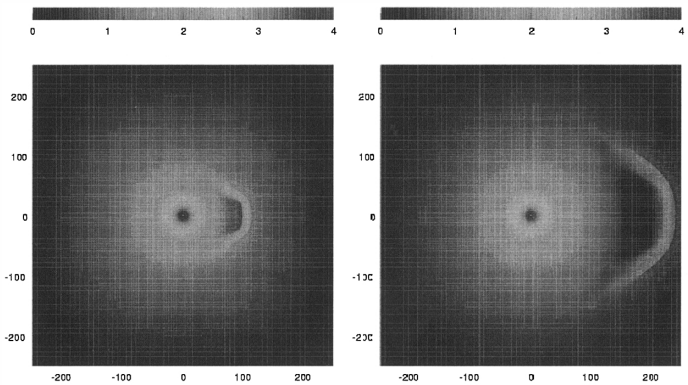

Fig. 1. Density distributions of model 1 on the solar equator plane at 24 (left) and 52 (right) hours after the occurrence of the CME. The logarithm of the density is expressed by the gray scale. The unit of length is the solar radius. The sun is located at the center (0,0,0). The horizontal axis faces the direction of the CME eruption. The earth is located at (195,91,0).

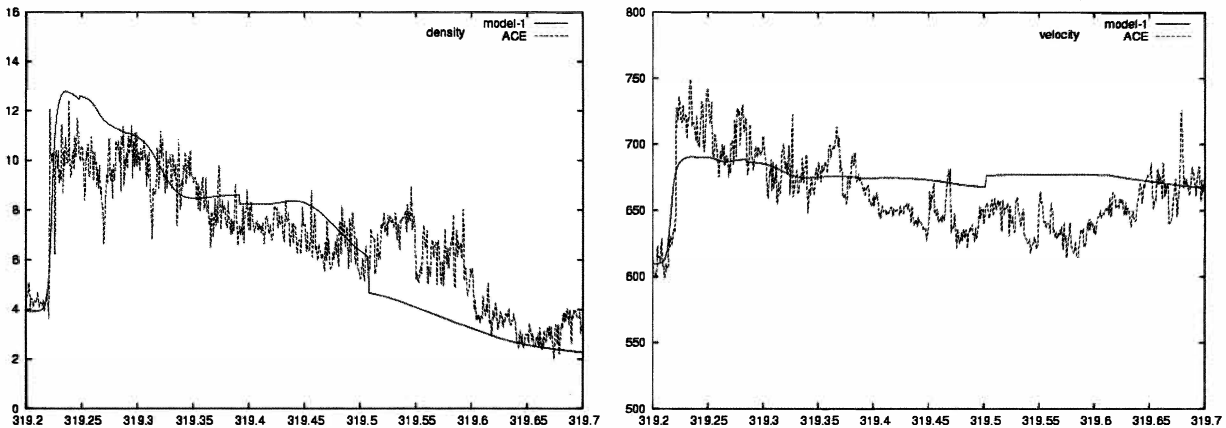

Fig. 2. Density plot (left) and velocity plot (right) for model 1 compared with the ACE data. The unit of the horizontal axis is Day of Year. The units of the vertical axes in the two panels are cm^{-3} (left) and km/s (right), respectively. The simulated results were adjusted so that the rise time coincided with the observed one.

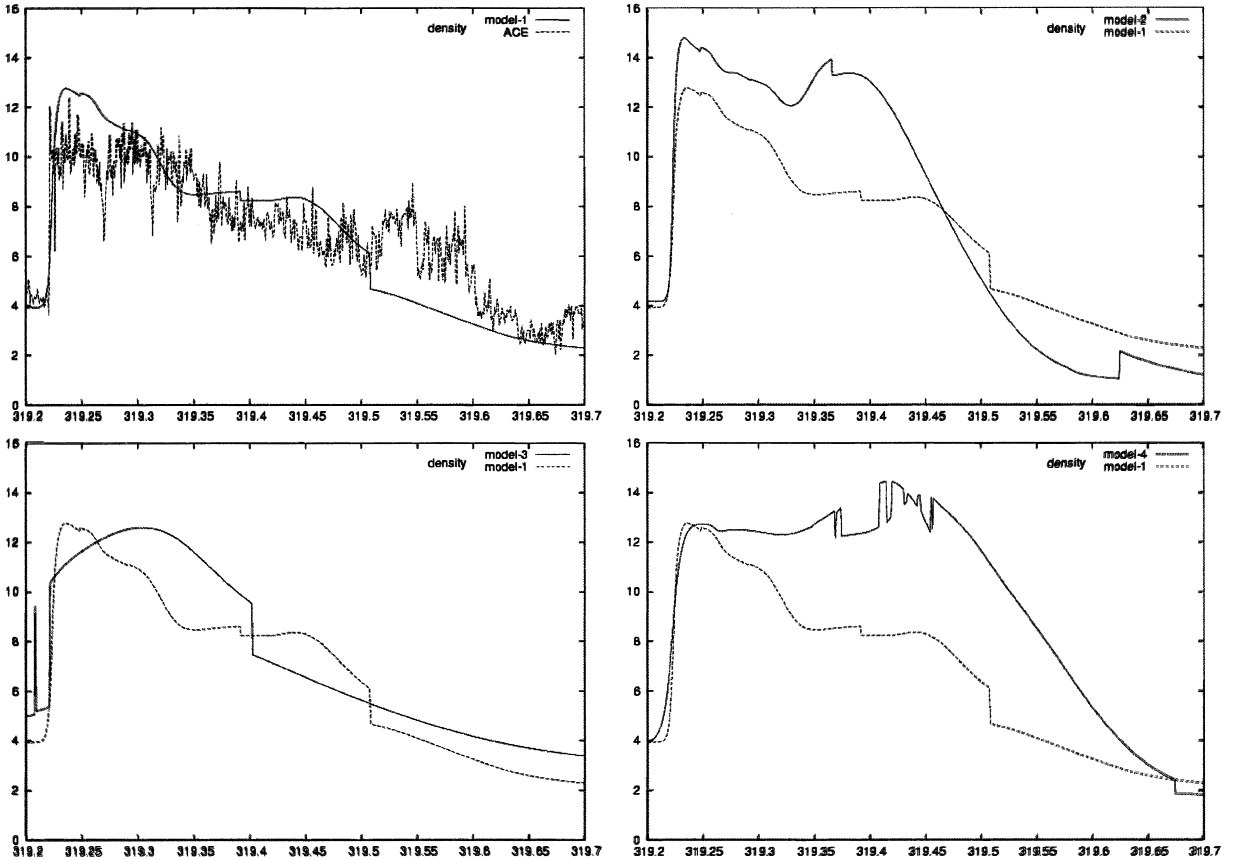

Fig. 3. Density plot of model 1 compared with the ACE data (upper left) and density plots of models 2–4 compared with that of model 1 (upper right, lower left, and lower right). The units of the horizontal and vertical axes are Day of Year and cm^{-3}, respectively. The simulated results were adjusted so that the rise time coincided with the observed one.

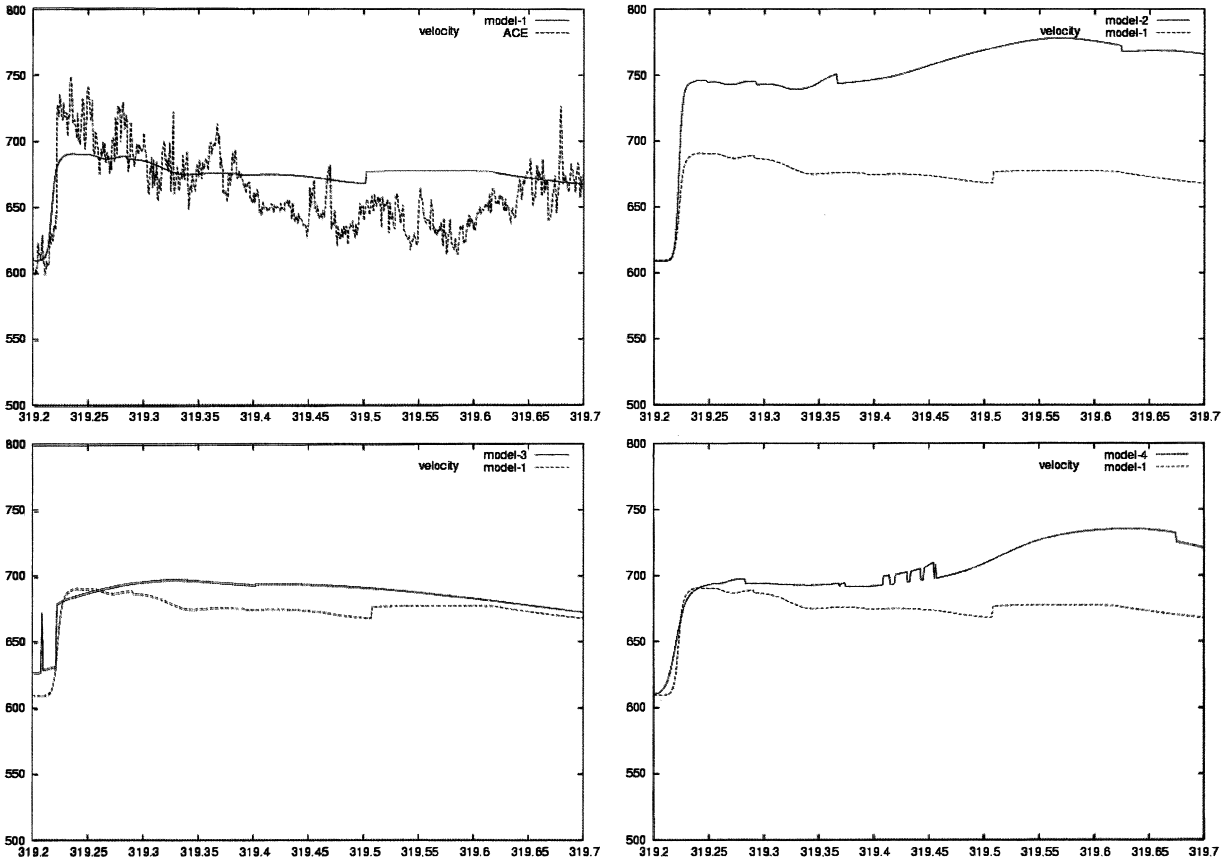

Fig. 4. Velocity plot of model 1 compared with the ACE data (upper left) and velocity plots of models 2–4 compared with that of model 1 (upper right, lower left, and lower right). The units of the horizontal and vertical axes are Day of Year and km/s, respectively.

model 3 was similar to model 1, but a bit higher. Model 4 erupted a low density for a long duration. The density plot of model 4 had a flat profile. In these plots, some discontinuous profiles with small jumps were observed. These apparent variations were caused by switching from fine cells to coarse cells at point L1, since the merging of the cells implies the movement of the observation point of the imaginary spacecraft, which was placed at the center of the cell nearest to the point L1.

5. Conclusions and discussion

We simulated an interplanetary shock wave caused by a CME that occurred at 0930 UT on November 13, 2003. A model with a temporal variation in the solar wind density at point L1 was fitted to the observations, and three other models were employed for comparison. Plots of the temporal variations in density and velocity at point L1 were then compared with the ACE data. The travel time of the shock wave in model 1 was 51.6 hours, 18% longer than the observed value of 43.8 hours. Our AMR code allocated $(0.24R_{\odot})^3$-sized cells to the region of the shock. This cell size corresponded to a resolution of 1/2048, making it possible to reproduce steep gradient of physical quantities for the shock. While a regular interval mesh of 2048^3 requires 8.6×10^9 cells, our simulation only used 1.8×10^7 cells. The elapse time of our simulation was about 11 hours, which is much shorter than the actual travel times of CME-caused shock waves. In the present paper, we showed that our simulation was able to characterize an interplanetary shock wave sharply and to reproduce the density fluctuations at point L1. Our AMR code also has the potential to predict the passage of a CME-caused shock wave.

Of note, the travel time in simulation was measured from the beginning of the CME input into the inner boundary, while the SOHO/LASCO data detected a CME when a bright loop appeared in the field of view. In general, a time lag of several tens minutes to a few hours May exist between these two measurements. However, the data in the LASCO CME Catalog suggested that the time lag of the CME was only about half an hour. This lag cannot explain the difference between the simulated travel times and the observed ones. Although the Joint USAF/NOAA Report states that the CME appeared to erupt off an east limb, the SOHO LASCO CME Catalog states that the CME was a partial halo with a diffuse angular width of 217 degrees. These records that the actual width of the CME was larger than Odstrcil and Pizzo's (1999) value of $\xi_0=15^\circ$, which we used in this study, and that the CME was located at a larger longitude in the east than our best fit value of E25°. A larger longitude and a wider diffusion value for the CME may account for the differences in the travel times. However, the location and diffusion of a CME are difficult to derive from observations. We believe that these parameters should be adjusted so that the solar wind variation at point L1 agrees with the observations.

The density plot of model 1 agreed well with the observations. On the other hand, the velocity plot of model 1 was flatter than the observations. We adopted a CME model that was similar to Odstrcil and Pizzo's model (Odstrcil and Pizzo, 1999). However, we placed the inner boundary at $1.1R_{\odot}$, very close to the sun surface, while Odstrcil and Pizzo placed the inner boundary at $30R_{\odot}$, distant from the sun. A different CME may be required when the inner boundary is set close to the solar surface.

The CME model should be improved to reproduce both density and velocity plots more accurately. Furthermore, the solar magnetic field may influence the evolution of CMEs. CME observations show a nearly constant velocity of the shock front from about $3R_\odot$ to $27R_\odot$ (see the SOHO LASCO CME Catalog). The magnetic effects on the shock front of the CME seem to be small, but they may affect the post-shock region. The effects of the solar magnetic field will be examined in our next study. Odstrcil and Pizzo (1999) and Odstrcil *et al.* (2004) demonstrated that interactions between a CME-caused shock wave and the ambient solar wind distort the shock front. In the present paper, we selected a CME that had a quiet pre-shock solar wind to allow this effect to be ignored. In general, a structured solar wind should be modeled in a simulation of an interplanetary shock wave propagation. In the future, we hope to introduce a realistic model of a solar magnetic field through which the solar wind structure can be reproduced.

Acknowledgments

Data from the SOHO LASCO CME Catalog was used in the present study. This CME catalog is generated and maintained by NASA and The Catholic University of America in cooperation with the Naval Research Laboratory. SOHO is an international cooperation between ESA and NASA. Data from the Joint USAF/NOAA Report of Solar and Geophysical Activity was also used. We are grateful for the production of these useful and well-ordered data.

The editor thanks Drs. M. Tokumaru and T. Nakagawa for their help in evaluating this paper.

References

Fujii, K. (1994): Numerical Methods for Computational Fluid Dynamics (Ryutai Rikigaku no Suchi Keisan-ho). Tokyo, University of Tokyo Press (in Japanese).

Khokhlov, A.M. (1998): Fully threaded tree algorithms for adaptive refinement fluid dynamics simulations. J. Comput. Phys., **143**, 519–543.

Manchester, W.B., Gombosi, T.I., Roussev, I., Ridley, A., De Zeeuw, D.L., Sokolov, I.V. and Powell, K.G. (2004): Modeling a space weather event from the Sun to the Earth: CME generation and interplanetary propagation. J. Geophys. Res., **109**, A02107.

Odstrcil, D. and Pizzo, V.J. (1999): Three-dimensional propagation of coronal mass ejections (CMEs) in a structured solar wind flow 1.CME launched within the streamer belt. J. Geophys. Res., **104** (A1), 483–492.

Odstrcil, D., Riley, P. and Zhao, X.P. (2004): Numerical simulation of the 12 May 1997 interplanetary CME event. J. Geophys. Res., **109**, A02116.

Roe, P.L. (1981): Approximate riemann solvers, parameter vectors, and difference schemes. J. Comput. Phys., **43**, 357–372.

Van Leer, B. (1977): Toward the ultimate conservative difference scheme. 4, A new approach to numerical convection. J. Comput. Phys., **23**, 276–299.

Van Leer, B. (1979): Toward the ultimate conservative difference scheme. 5, A second-order sequel to Godunov's method. J. Comput. Phys., **32**, 101–136.